Running head: SPATIOTEMPORAL FMRI-CPCA

# Combining temporal and spatial constraints in task-based fMRI

Meighen M. Roes[1,2]

Yoshio Takane[3]

&

Todd S. Woodward[2,4*]

[1]Department of Psychology, University of British Columbia, Vancouver, BC, Canada.

[2]BC Mental Health and Substance Use Research Institute, Provincial Health Services Authority, Vancouver, BC, Canada.

[3] Department of Psychology, University of Victoria, Victoria, Canada

[4]Department of Psychiatry, University of British Columbia, Vancouver, BC, Canada.

*Corresponding author. Please address correspondence to Todd S. Woodward, Ph.D., BC Mental Health and Substance Use Research Institute, Room 117, 3rd Floor, 938 W. 28th Avenue, Vancouver, B.C., Canada. V5Z 4H4. E-mail: todd.woodward@ubc.ca. Phone: 604-875-2000 x 4724. Fax: 604-875-3871.

Abstract: 247 Body: 4961

KEY WORDS: fMRI/connectivity/fMRI-CPCA/hemodynamic response/task-based/networks

Abstract

**Introduction.** Constrained principal component analysis for fMRI (fMRI-CPCA) is carried out in two main steps: (1) blood-oxygen-level dependent (BOLD) signal is row (time)-constrained to variance predictable from a finite impulse response (FIR) model, and (2) task-based networks and their associated estimated hemodynamic response shapes (HDR) are extracted through dimension reduction. In the current study, we introduce a novel methodology that additionally employs *anatomical patterns as constraints on columns* (voxels). We refer to this as spatiotemporal fMRI-CPCA (ST-fMRI-CPCA).

**Methods.** In a series of analyses, we tested whether ST-fMRI-CPCA accurately portions the row (time)-constrained variance into that which is predictable (and not) from network-level constraints on columns (voxels). This was achieved by (1) preserving the networks retrieved from a traditional row-constrained fMRI-CPCA, and (2) systematically including or excluding these networks from column constraints to test whether they are retrievable in the portions of row (time)-constrained variance that are predictable (or not) from the column constraints. Retrieval of a network was determined anatomically through spatial correlation, and temporally through analysis of HDR shapes.

**Results.** Our analyses validate ST-fMRI-CPCA as a method that can separately retrieve task-based brain networks, and their associated HDRs, from spatial-model-predictable and spatial-model-unpredictable aspects of task timing-related fluctuations in BOLD signal.

**Conclusion.** ST-fMRI-CPCA is an accurate tool for evaluating network models as predictors of BOLD signal changes induced by task-based fMRI and could be employed to compare spatial models (e.g., parcellations or competing network sets) on their ability to account for the task-timing-related brain networks measurable by fMRI.

**Impact Statement:**

ST-fMRI-CPCA is a novel tool for combining temporal and spatial constraints to retrieve brain networks from task-based fMRI data. It can be used to compare spatial models by exploring the degree to which competing spatial models can capture task timing-predictable variance in BOLD signal. Applications include comparison of parcellation schemes, or network sets, for explaining task-based fMRI data.

## Combining temporal and spatial constraints in task-based fMRI

Constrained Principal Component Analysis for fMRI (fMRI-CPCA) has emerged as a reliable data-driven method for extraction of task-based brain networks from fMRI data, including their associated hemodynamic response shapes, which are interpreted to determine cognitive functions (e.g., Damascelli et al., 2021; Larivière et al., 2017; Lavigne, Menon, Moritz, & Woodward, 2020; Lavigne, Metzak, & Woodward, 2015; Metzak et al., 2011; Metzak et al., 2012; Roes, Chinchani, & Woodward, 2021; Sanford, Whitman, & Woodward, 2020; Whitman, Metzak, Lavigne, & Woodward, 2013; Wong et al., 2020; Woodward et al., 2006; Woodward et al., 2015). In its standard application, prior to dimension reduction, variability in blood oxygen level dependent (BOLD) signal is constrained to that portion which is predictable from task timing for the specific task under study. Importantly, fMRI-CPCA uses a finite impulse response (FIR) model (Lindquist, Meng Loh, Atlas, & Wager, 2009) which does not make a priori assumptions that networks exhibit a canonical HDR shape, but instead estimates the HDR shape from the data. This practice acknowledges that the shape of the HDR may be task-, condition, and subject-specific; observation of HDR timing, and responses to tasks and task conditions, is the primary way to identify the cognitive process(es) supported by each functional network. Spatial characteristics of the networks, in the form of component loadings overlaid onto a brain image to visualize the voxels most strongly contributing to each functional network, provide a supporting basis for the cognitive process(es) derived from the HDRs. Because this form of fMRI-CPCA is spatially exploratory, with no anatomical models or parcellation schemes, we refer to it as the “data-driven” fMRI-CPCA method.

CPCA as a general statistical technique provides a highly flexible framework for examining the structure of multivariate data as it relates to auxiliary information about the rows and/or columns of a data matrix (Takane & Shibayama, 1991), and although row-wise

constraints (timing) and column-wise (spatial) constraints have separately been exploited, the simultaneous application of *both* kinds of constraints is also possible for fMRI data analysis (Takane & Shibayama, 1991). Task timing constraints (a row-wise constraint only), are the basis of the 'data-driven' fMRI-CPCA model, whereas spatial/voxel constraints (a column-wise constraint- e.g., regions or network models of interest) have separately used to translate fMRI networks into the domain of MEG, for example (Metzak, 2017; Whitman et al., 2016). In the context of task-based fMRI data analysis with CPCA, combining row and column constraints would enable BOLD signal variance to be partitioned into four orthogonal partitions: that which is predictable from task timing in conjunction with a spatial model of interest (SMoI), that which is predictable from task timing but orthogonal to the SMoI, that which is predictable from the SMoI but orthogonal to task timing, and that orthogonal to both task timing and the SMOI (i.e., error). Dimension reduction can be applied to any or all of these orthogonal sources of variance. Those partitions of variance involving the combination of row and column constraints (i.e., those predictable from task timing and SMoIs simultaneously) provide the basis for evaluating spatial models as predictors of the BOLD signal changes induced by task-based fMRI.

fMRI-CPCA with combined temporal and spatial constraints would enable, for example, comparison of resting-state to task-based functional networks (e.g, Bzdok et al., 2016; Yeo et al., 2015), various parcellation methods (Bellec, Rosa-Neto, Lyttelton, Benali, & Evans, 2010; Glasser et al., 2016; Gordon et al., 2016; Schaefer et al., 2018; Yeo et al., 2011), or overlapping task-based network models (e.g., Fedorenko, Duncan, & Kanwisher, 2013; Percival, Zahid, & Woodward, 2020; Yarkoni, Poldrack, Nichols, Van Essen, & Wager, 2011) as predictors of the dominant dimensions of BOLD signal related to task timing. Additionally, such a method may reduce the need to classify retrieved networks in the absence of SMoIs, by directly providing the weightings of networks retrieved as one of the outputs when combining row with column constraints.

The objective of the present study is to confirm the ability of simultaneous timing (row) and spatial (column) constraints to retrieve brain networks that are known to be involved in task-based fMRI, because they were previously retrieved by the standard row-constrained fMRI-CPCA. This application of fMRI-CPCA is referred to as spatiotemporal fMRI-CPCA (ST-fMRI-CPCA). Here, we introduce the technical details regarding the ST-fMRI-CPCA methodology and present a series of analyses that validate this approach and demonstrate the metrics by which spatial models can be evaluated as predictors of the network-level BOLD signal changes induced by task-based fMRI. We discuss the implications and applications of this approach for task-based fMRI data analysis.

## Methods

Constrained Principal Component Analysis (CPCA) is a general technique that combines regression analysis and principal component analysis into a unified framework (Takane & Shibayama, 1991), revealing dimensions of the data that are optimally predicted by external information about the rows and/or columns of the data. Generally speaking, CPCA is carried out in two steps: 1) External information about the rows (full brain scans or TRs in the case of fMRI-CPCA) and/or columns (voxels in the case of fMRI-CPCA) of the data matrix are used as predictors in column-wise and/or row-wise multivariate multiple regressions. The resulting regression model partitions the total variability in the dataset into that which can be predicted from row and/or column predictor variables, and that which cannot (referred to as matrices of error scores in the tradition of multiple regression). 2) Next, PCA is performed on the resulting constrained matrices (referred to as matrices of predicted scores in the tradition of multiple regression) to determine patterns of inter-correlations within the data related to row and/or column predictor variable matrices. For an introduction to the theory and the diverse applications of CPCA, see Takane & Shibiyama (1991), Takane & Hunter (2001), and Hunter & Takane (2002). In the context of fMRI data analysis, the data matrix consists of the full array of task-fMRI data, as is described below.

**Data matrix (*Z*) of Dependent Variables**

The 2-dimensional data matrix, $Z$, contains the full time series of fMRI scans for all subjects ($n \times s$ rows) for all voxels of interest in the brain ($m$ columns), where $n$ is the number of subjects, $s$ is the number of full-brain scans in the time series, and $m$ is the number of voxels after masking out non-brain areas, realigned, smoothed, and spatially normalized, mean-centered and standardized to a variance of 1.0 prior to further analysis. The construction of the $Z$ matrix in this fashion, with time-series information about the BOLD signal in the rows, and spatial/voxel information in the columns, allows the use of task-timing (row) and/or spatial (column) constraints to examine specific portions of BOLD variance related to task-timing and/or models of interest.

**Row-wise Independent Variables (*G*)**

The design matrix $G$ contains the timing information for the fMRI experiment, where each row of $G$ corresponds to a whole-brain scan in the data matrix $Z$. $G$ contains a FIR model specifying the post-stimulus time points for which changes in BOLD signal relative to all other scans are to be estimated in a data-driven fashion (Henson, Rugg, & Friston, 2001; Serences, 2004). The columns in the subject- and condition-based $G$ matrix encode the $t$ peristimulus time points for each experimental condition, for each subject, totaling $n \times k \times t$ columns in $G$, where $n$ is the number of subjects and $k$ is the number of conditions. The value 1 is placed in the rows of $G$ for which BOLD signal amplitude is to be estimated, and 0's are placed in all other rows.

In a spatially 'data-driven' fMRI-CPCA analysis, BOLD signal is constrained solely by task timing information represented in the $G$ matrix, as detailed previously elsewhere (Metzak et al., 2011; Metzak et al., 2012) and in the Supplementary material. Briefly, in a data-driven fMRI-CPCA analysis, $Z$ is regressed onto the task timing/design matrix ($G$) to produce the $GC$ matrix containing the BOLD signal predictable from the timing of stimulus presentations, and $E$ (error),

$$Z = GC + E. \quad (1)$$

Following this, the dominant dimensions of task timing-related variance ($GC$) are characterized through PCA.

**Column-wise Independent Variables (*H*)**

The novelty and usefulness of ST-fMRI-CPCA is that it further partitions task-timing predictable variance ($GC$) into SMoI -predicted and -unpredicted sources of task-timing related variance. In ST-fMRI-CPCA, the $H$ matrix specifies the SMoI that will be used to constrain variance in measured BOLD signal over columns. The $H$ matrix has $m$ rows, each one corresponding to a voxel represented in the analysis (i.e., a column of $Z$). Column-wise constraints optimize results to those predictable from the voxel-wise information, such as brain network patterns, parcellation schemes, or hypothesized spatial contrasts. For example, using an SMoI in $H,$ one could constrain results to a contrast of hemispheres, or probe the degree to which hypothesized voxel-wise brain network patterns account for variance in BOLD signal; see Figure 2 for an illustration of $H$ matrix creation.

**Spatiotemporal fMRI-CPCA Step 1: Multivariate multiple regression**

The full form of the CPCA model is as follows:

$$Z = GMH' + GC_{notH} + B_{notG}H' + E, \quad (2)$$

where $Z$, $G$, and $H$ are the BOLD signal data matrix, temporal model, and SMoI matrices previously described, respectively. In the multivariate multiple regression step of ST-fMRI-CPCA, $G$ and $H$ are used as row-wise and column-wise independent variables, respectively. This allows fMRI BOLD signal variance to be partitioned into the portion predictable from task timing in conjunction with the SMoI ($GMH'$), predictable from task timing independent of the SMoI ($GC_{notH}$), the portion the portion predictable from the SMoI but not from task timing ($B_{notG}H'$), and error ($E$). Thus, it provides a basis upon which to explore the performance of different network models in predicting task-timing-dependent brain activity.

In the above equation, $GMH'$ represents the portion of $Z$ that can be explained by the combination of both $G$ and $H$. Relative to the $GC$ matrix from a 'data-driven' fMRI-CPCA, which is already constrained by the temporal model, $GMH'$ represents the subset of BOLD signal that is also predicted by the SMoI. The matrix of regression coefficients, $M$, is estimated as follows:

$$Z = GMH' + GC_{notH} + B_{notG}H' + E, \quad (3)$$

$GC_{notH}$ represents the portion of $Z$ that can be explained by $G$ independent of $H$. In ST-fMRI-CPCA, it represents task-timing-predictable BOLD signal variance that is not explained by the SMoI. The parameter $C_{notH}$ contains regression weights for each scan timepoint, and is estimated by regressing $Z$ onto that part of $G$ that is independent of $H$, as follows:

$$C_{notH} = (G'G)^{-1} \times G'Z \times [I_m - H \times (H'H)^{-1} \times H'], \quad (4)$$

where $I_m$ is an identity matrix sized on the columns of $Z$ (voxels) that contains ones on the main diagonal and zeros elsewhere.

Because our focus here is on task-timing related activity, details regarding the computation and characterization of task timing-unpredicted portions of variance ($B_{notG}H'$ and residual variance, $E$) will not be discussed here, but have been explained in more detail in the Supplementary Material.

### 1.1.1 Spatiotemporal fMRI-CPCA Step 2: Principal Component Analyses.

PCA can be applied separately to each of the matrices resulting from the multivariate regression step (viz., $GMH$, $GC_{notH}$, $B_{notG}H'$, and $E$) in order to examine the structure of specific portions of BOLD signal variance that are of interest, which are orthogonal, so can be interpreted independently. In the application described here, the task-timing-predictable variances in BOLD signal that can (i.e., $GMH'$) or cannot (i.e., $GC_{notH}$) be explained by a specified SMoI $H$ are of primary interest.

The matrix $GMH'$ (activations predicted by task timing in conjunction with the SMoI) is decomposed using singular value decomposition (SVD) as follows:

$$UDV' = GMH'. \quad (5)$$

The left singular values of $GMH'$ correspond to time-series information about the components, and the right singular vector $V$ contains spatial information about the components. Because $GMH'$ is predictable from both task-timing (row) and spatial (column) information, we can compute predictor weights describing the contribution of both the SMoI ($P_H$) and task-timing information ($P_G$) to each spatiotemporal component. $P_H$ predictor weights are the unstandardized beta coefficients produced by regressing the right singular vector $V$ of $UDV'$= $GMH'$ onto $H$;

$$P_H = (H'H)^{-1} \times H'V. \quad (6)$$

The $P_H$ weights computed using the above equation specify how the columns of $H$ linearly recombine to produce the $GMH'$ component images. Therefore, where a network from a SMoI perfectly corresponds to a $GMH'$ component image, that network will have a predictor weight of magnitude 1, and all other networks included in the model will have a predictor weight of 0.

$P_G$ predictor weights provide subject- and condition-specific HDR estimates for each $GMH'$ component, and are the unstandardized beta coefficients produced by regressing the left singular vector $U$ of $UDV'$= $GMH'$ onto $H$;

$$P_G = (G'G)^{-1} \times G'U. \quad (7)$$

The matrix $GC_{notH}$ can also be characterized to examine the task-related variance in BOLD signal that is not captured by a SMoI. $GC_{notH}$ is decomposed through SVD:

$$UDV' = GC_{notH}. \quad (8)$$

Interpretation of $GC_{notH}$ components proceeds in much the same way as in a data-driven fMRI-CPCA. $P_{GnotH}$ predictor weights provide subject- and condition-specific HDR estimates for each $GC_{notH}$.component, and are computed as the unstandardized beta coefficients produced by regressing the left singular vector $U$ of $UDV'$=$GC_{notH}$ onto $H$. Component loadings provide spatial information about each $GC_{notH}$.component. Conceptually, $GC_{notH}$ components describe spatiotemporal aspects of task-related networks that are not accounted for by the SMoI.

**Spatiotemporal fMRI-CPCA test case selection**

The mathematical proof for CPCA with combined column-wise and row-wise constraints has been published previously as a general methodology (Takane & Shibayama, 1991); however, the current study is the first to implement this model for the purpose of fMRI data analysis. Therefore, our aim was to test whether ST-fMRI-CPCA accurately portions the row (time)-constrained variance into that which is predicted (and not) by the network-level constraints on columns (voxels). Our second objective is to demonstrate the metrics by which network model performance can be evaluated using this method.

We first identified 'test cases' for which the expected outcomes were known, based on the relations between $GC$, $GMH'$ and $GC_{notH}$, as illustrated in Figure 1. Namely, in a ST-fMRI-CPCA, all task-timing related variance (i.e., the $GC$ variance in a spatially "data-driven" fMRI-CPCA with timing constraints only) is further subdivided into spatial-model-predicted ($GMH'$) and spatial-model-unpredicted ($GC_{notH}$) task timing-related variance; that is, $GC = GMH' + GC_{notH}$. It logically follows that where a SMoI *H* perfectly predicts all task-timing related variance, then $GC = GMH'$, and $GC_{notH} = 0$. Where a SMoI (i.e., linear recombination of the networks specified in $H$) fails to predict task timing-related variance, the residual variance instead should be retrievable in $GC_{notH}$, the portion of variance that is related to timing constraints, but is SMoI -independent.

We can make use of the relationships illustrated in Figure 1 to engineer test cases for which the expected structure of $GMH'$ and $GC_{notH}$ have already been derived from "data-driven" $GC$ component loadings, which are by definition redundant with timing constraints. Any data-driven networks (i.e., whole-brain images of the original $GC$ components) that are included in the SMoI $H$ should be retrieved in $GMH'$; any data-driven networks that are excluded from the SMoI $H$ will be retrieved from $GC_{notH}$. In these scenarios, the spatiotemporal features and variance explained by the data-driven networks should be exactly replicated in the structure of

either $GMH'$ (for those data-driven networks included in the SMoI) or $GC_{notH}$ (for those data-driven networks omitted from the SMoI).

Based on this logic, three test cases were planned, using the data and networks reported in a recently published data-driven fMRI-CPCA analysis of external data that derived three networks (a Language/Attention network – LANG/ATTN, a Responding network - RESP, and the default mode network - DMN), each of which showed hypo-activation among patients with schizophrenia relative to healthy controls during successful paired associates encoding, but not unsuccessful encoding or a control condition.

In Test Case 1, we placed all three of these data-driven networks (RESP, LANG/ATTN, DMN) in the SMoI $(H)$, to verify that $GMH'$ accurately captures combined SMoI- and task-timing-predicted networks. In Test Case 2, we placed all but one of the data-driven networks (DMN) in our SMoI to verify that $GC_{notH}$ accurately captures task-timing-predictable brain networks that are *not* accounted for by the SMoI. Finally, in Test Case 3, we verified that our program correctly specifies how networks in $H$ linearly recombine to estimate the spatial features of task-timing related networks (the $GMH'$ component images).

Together, these test cases were designed to verify that our program for ST-fMRI-CPCA successfully characterizes SMoI -predicted and -unpredicted sources of task-timing-predictable variance in BOLD signal, and to demonstrate how the performance of different models as predictors of task-based networks can be evaluated using ST-fMRI-CPCA.

**Test case data**

The test case data matrix $Z$ and design matrix $G$ have already been described in Roes et al., (2021). Briefly, the $Z$ matrix contained BOLD intensity values for 76470 voxels over 80 × 242 = 3,660 preprocessed scans (80 subjects with 242 scans each). The columns in the subject- and condition-based $G$ design matrix coded 10 post-stimulus time points for each of the encoding conditions (successful encoding, unsuccessful encoding, and control condition) for

40 persons with schizophrenia and 40 age- and gender-matched healthy controls, totaling 3,660 columns in $G$. In the original analysis, 17.50% of overall BOLD signal was predictable from task timing, and a portion of this overall BOLD signal variance was related to coherent network activity. We extracted.three data-driven networks (a responding network; RESP, a language/attention network; LANG/ATTN, and the default mode network; DMN) that accounted for 18.50%, 12.97%, and 8.02% of the task-timing related variance in BOLD signal, respectively, and which together accounted for 6.83% of overall BOLD signal variance. The images for these data-driven $GC$ components were retained for testing of our ST-fMRI-CPCA program.

**Test Case *H* matrix construction**

*Test Case 1*

In test case 1, the SMoI contained all three of the data-driven networks. To construct the $H$ matrix, the component loadings for each data-driven network were converted into a vector of 76,470 × 1 and horizontally concatenated to produce a 76,470 × 3 matrix.

*Test Case 2*

Test case 2 was designed to verify that ST-fMRI-CPCA analysis would correctly characterize model-*unpredicted* sources of task timing-related variance. Therefore, in test case 2, we included only two of the data-driven networks (RESP and LANG/ATTN) in our SMoI, omitting the DMN. As a result, the $H$ matrix for test case 2 contained 76,470 rows and 2 columns.

*Test Case 3*

Test case 3 was designed to verify the computation of, and illustrate the meaning of, the $P_H$ weights. $P_H$ weights specify how the networks from $H$ linearly recombine to produce the $GMH'$ component loadings, which represent the SMoI-predicted spatial characteristics of task timing-related networks. As in the other test cases, since the data-driven networks had already

been measured, we could specify a SMoI in $H$ that would produce perfect $GMH'$ estimates of the data-driven networks. In this test case, we did this by building the $H$ matrix from a set of pseudo-networks that linearly recombined, using pre-specified weights, into the three data-driven networks (See Figure 3), with the expectation that the $P_H$ weights will correspond to these pre-specified values.

To create the first two columns of the spatial model $H$ for test case 3, the RESP network was split into two spatially non-overlapping pseudo-networks $A$ and $B$. Pseudo-network $A$ contained the natural $GC$ loadings for the left hemisphere, and Pseudo-network $B$ contained the natural loadings for the right hemisphere of the RESP network, with all other values set to zero, so that $RESP = (1.0 \times A) + (1.0 \times B)$.

For the third and fourth columns of the $H$ matrix, in order to provide an illustration involving negative $P_H$ spatial model weights, we created Pseudo-networks $C$ and $D$ such that $LANG/ATTN = (1.00 \times C) + (-1.00 \times D)$ (See Supplement for details on Pseudo-network creation).

For the fifth and sixth columns of the $H$ matrix, we created two final Pseudo-networks, $E$ and $F$, that linearly recombined in a *weighted* manner to produce the natural loadings of the *DMN,* $DMN = (1.25 \times E) + (0.25 \times F)$ (See Supplement for details). Here, note that the $P_H$ weights need not be, or sum to, 1.00. They are not correlations of the respective columns of $H$ with the $GMH'$component loadings. Instead, they represent how the respective columns of the $H$ matrix are weighted so that their sum produces the right singular vector of $GMH'$.

As a result, the $H$ matrix for test case 3 contained 76470 rows and 6 columns (Pseudo-networks *A* through *F*). Because each data-driven network could be perfectly described using weighted combinations of the columns of $H$, this analysis was expected to produce three $GMH'$ components corresponding to the RESP, LANG/ATTN, and DMN. In this test case, the $P_H$ weights should correspond to those weights that we pre-specified to produce the original

data-driven networks from known linear combinations of the columns of $H$ [e.g., for the RESP network, the six columns of $H$ should have $P_H$ weights of 1.0, 1.0, 0.0, 0.0, 0.0, and 0.0, respectively; See Figure 3)]

**Model performance metrics:**

For each test case, a ST- fMRI-CPCA analysis was carried out as previously described; briefly, in the regression stage, total variance in BOLD signal was partitioned into $GMH'$, $GC_{notH}$, and task-unrelated variance. PCA was then conducted on the $GMH'$ and $GC_{notH}$ matrices, producing both spatial and timing information for each component extracted from the model-dependent ($GMH'$) and model-independent ($GC_{notH}$) sources of task timing-related variance.

SMoI performance can then be evaluated using ST-fMRI-CPCA by examining the degree to which the SMoI captures task timing-related variance, produces an accurate estimate of the spatial configuration of task timing-related networks, and captures the features of the networks' hemodynamic response. $P_H$ weights specify how the networks in $H$ linearly recombine to produce the $GMH'$ components (i.e., the estimates of the data-driven task timing-related networks). Each of these metrics is expanded on below in the context of our test case analyses.

**Metric 1: Capture of task timing-related variance**

The first metric of model performance is the degree to which it captures task timing-related variance in BOLD signal. We generated test cases where the SMoI was redundant with timing constraints, while excluding some networks from the column-constraints to test whether they are retrievable in the portion of row (time)-constrained variance that is not predictable from the column constraints. Therefore, in our test cases, 100% of the task timing-related variance attributable to any data-driven networks included in the SMoI specified in $H$ should be captured in $GMH'$, whereas 100% of task timing-related variance related any data-driven networks omitted from the SMoI should instead appear in $GC_{notH}$

**Metric 2: Prediction of Spatial Characteristics**

The second metric of model performance is the degree to which it accurately retrieves the spatial configuration of task timing-related networks. Spatial correspondence is measured through spatial correlation. In the current test case analyses, the principal component loadings of $GMH'$ should perfectly spatially replicate those of any data-driven $GC$ networks that were included in the SMoI, whereas the principal component loadings of $GC_{notH}$ should perfectly spatially replicate any $GC$ networks that were excluded from the SMoI. Where there is an exact spatial correspondence, there will be a perfect correlation ($r$ = 1.00) between the loadings of $GC$ and $GMH'$ (for any data-driven networks included in $H$) and between the loadings of $GC$ and $GC_{notH}$ (for any data-driven networks omitted from $H$).

**Metric 3: Prediction of Hemodynamic Characteristics**

The third criterion for model performance is the extent to which the model accurately estimates the HDR features of the data-driven networks. In our test case analyses, the temporal characteristics of the original $GC$ components should therefore be exactly replicated, either in $GMH'$ or $GC_{notH}$(depending on whether the $GC$ network was included or omitted from the SMoI, respectively). Operationally, there should be a perfect correspondence of the HDRs of the $GMH'$ components with any $GC$ networks modeled in $H$. Further, any differences in network HDR between patients and healthy controls, or as a function of time or task condition, should be preserved in the relevant portion of SMoI-predicted or -unpredicted variance in task-related BOLD signal.

**Linear recombination of spatial model networks to estimate task-based networks (spatial model weights, $P_H$ ):**

The $P_H$ predictor weights are equivalent to unstandardized beta coefficients, and they specify how the networks included in $H$ linearly recombine to estimate the spatial features of the task-timing related networks. In Test Cases 1 and 2, as a consequence of the expected exact

spatial match between $GMH'$ components with our original data-driven networks, the $P_H$ predictor weights should have a magnitude of |1.0| for the match between each data-driven component included in $H$ and its $GMH'$ counterpart. In Test Case 3, the $P_H$ weights should correspond to the weights (See Figure 3) that when applied to the columns of $H$ reconstitute the original data-driven networks.

## Results

**Test Case 1 (all data-driven networks in *H*):**

Figure 4 summarizes the results of Test Case 1. As expected, the $GMH'$ scree plot indicated that 3 task-timing and SMoI-predicted components be retained, accounting for 18.50%, 12.97%, and 8.02% of BOLD signal variance, which equal the variances attributable to each of the original data-driven components. $GMH'$ component images for test case 1. As expected, there was a spatial correlation of $r$ = 1.00, indicating perfect spatial match between the $GMH'$ components and the data-driven networks they estimated. The HDRs are also presented in Figure 4; the temporal features of the modeled networks were also confirmed, and all Group, Time, and Encoding effects were reproduced exactly (omitted here for brevity – see Roes et al., 2021). Finally, as predicted, the $P_H$ predictor weights specifying the relation of each data-driven network in $H$ and its $GMH'$ component had a value of 1.00; all other $P_H$ predictor weights had a value of zero.

**Test case 2 (Two data-driven networks in *H*, DMN omitted from *H*)**

Figure 5 summarizes the results of test case 2. The $GMH'$ scree plot indicated that two components be extracted, and the $GC_{notH}$ scree plot indicated that one SMoI-unpredicted task timing-related component be retained. The spatial, variance, and temporal characteristics of the three components exactly corresponded to those of the data-driven RESP, LANG/ATTN and DMN. The only difference with the outcome of test case 1 was that, when we omitted the DMN

from the SMoI, the DMN was instead measured in $GC_{notH}$, the portion of task timing-related variance not predicted by the SMoI.

**Test case 3 (*H* consists of images that linearly recombine into the data-driven RESP, LANG/ATTN and DMN)**

Figure 6 summarizes the results of test case 3. Again, this test case produced $GMH'$ components corresponding to the RESP, LANG/ATTN and DMN, identical with regard to variances and spatiotemporal features as those found in test case 1. The main objective of this test case was to verify and illustrate that $P_H$ values specify how the columns of the SMoI *H* linearly recombine to estimate each task timing-related network. As expected, for the $GMH'$ component corresponding to the RESP network, Pseudo-networks *A* and *B* had $P_H$ predictor weights of 1.00 and 1.00, with all other model weights equaling zero. For the $GMH'$component corresponding to the LANG/ATTN network, the $P_H$ predictor weights had values of 1.00 and -1.00 for Pseudo-networks *C* and *D*, and the other pseudo-networks had $P_H$ predictor weights of zero. Finally, the $GMH'$ component corresponding to the DMN had $P_H$ predictor weights of 1.25 and 0.25 for Pseudo-networks *E* and *F*, with all other $P_H$ predictor weights equal to zero. These $P_H$ predictor weights were precisely those that we pre-specified as the weights that are applied to the pseudo-networks in order to linearly recombine into each data-driven network, validating the computation of $P_H$ predictor weights in ST-fMRI-CPCA program.

## Discussion

Constrained principal component analysis for fMRI (fMRI-CPCA) has emerged as a reliable data-driven method for measuring task-based networks and their associated hemodynamic response shapes. We introduce spatiotemporal fMRI-CPCA (ST-fMRI-CPCA), an extension of 'data-driven' fMRI-CPCA, for testing or comparing network models as predictors of the BOLD signal changes induced by task-based fMRI. A series of analyses systematically varied network models to either capture or omit known dimensions of task timing-related

variance. Three test cases demonstrated that our ST-fMRI-CPCA program correctly characterizes SMoI-dependent and –independent sources of task timing-related variance in BOLD signal. Examination of variance capture, spatial correspondence using spatial correlation of component loadings, temporal characteristics using HDR estimates, and $P_H$ predictor weights support these conclusions.

These test cases also illustrate the metrics that can be used to test the performance of different SMoIs in accounting for task-based functional networks. An ideal model of task-based brain networks would perfectly capture the temporal, spatial, and variance characteristics of data-driven networks. Test case 3 illustrates how $P_H$ predictor weights specify how the networks included in a SMoI linearly recombine to estimate the spatial features of task-based networks.

**Limitations**

The test case analyses reported here served to validate the computation only of task-timing related components of variance ($GMH'$and $GC_{notH}$). The variance related to SMoIs but not task timing, $B_{notG}H'$, was not assessed. Since task-timing independent variance can be conceived of as conceptually equivalent to 'resting state' (Arfanakis et al., 2000), further developing this method to separately characterize task timing-predicted versus -unpredicted networks, and their time-courses, would provide a new methodology in the ongoing efforts to understand how/whether 'intrinsic' connectivity shapes and informs task-based network activity.

**Future directions and applications**

The extension of fMRI-CPCA that is demonstrated here has several important applications in functional neuroimaging research. For example, this method could be used to investigate the theory that task-based networks represent a 'rebalancing' of resting state networks for task conditions (Bzdok et al., 2016; Krienen, Yeo, & Buckner, 2014). Moreover, it allows for comparison between different resting state network models (e.g., Smith et al., 2009; Smith et al., 2012; Yeo et al., 2011), parcellation methods (Arslan et al., 2018), or task-based network models (e.g., Percival et al., 2020; Yarkoni et al., 2011) as predictors of task-timing

related brain networks. Finally, should a researcher wish to classify task-based networks according to a pre-specified model, ST-fMRI-CPCA would provide an automated way to do, via examination of $P_H$ predictor weights.

**Conclusions**

Our test case analyses validate ST-fMRI-CPCA as a method that can separately retrieve networks, and the associated HDRs, from spatial-model-predictable and model-unpredictable aspects of task timing-related fluctuations in BOLD signal. ST-fMRI-CPCA can be used to compare different network or parcellation models as predictors of the spatiotemporal features of task-based networks.

**Acknowledgments**

The authors gratefully acknowledge John Paiement, who developed the original fMRI-CPCA program, and Ryan Lim and Hafsa Binte Zahid, who updated the program to incorporate ST-fMRI-CPCA capabilities. The analyses reported in this manuscript make secondary use of data originally collected as part of the UCLA Consortium for Neuropsychiatric Phenomics LA5c Study (Poldrack et al., 2016). The fMRI task data were obtained from the OpenfMRI database (https://openfmri.org/dataset/ds000030, accession number ds000030), as reported in Roes et al., (2021).

**Authorship Confirmation Statement**

The authors confirm contribution to the paper as follows: study conception and methodology: Meighen M. Roes, Yoshio Takane,Todd S. Woodward; analysis and interpretation of results: Meighen M. Roes, Todd S. Woodward; draft manuscript preparation: Meighen M. Roes, Todd. S. Woodward. All authors reviewed the results and contributed to manuscript revision and editing.

**Author Disclosure Statement**

The authors declare that there is no conflict of interest.

**Funding Statement**

This project was supported through a BC Children's Hospital Research Institute Trainee Boost Award to M. M. R, and through the Necia Elvin Memorial Prize for Schizophrenia Research to M. M. R., generously funded by Dr. Memory Elvin-Lewis.

## References

Arfanakis, K., Cordes, D., Haughton, V. M., Moritz, C. H., Quigley, M. A., & Meyerand, M. E. (2000). Combining independent component analysis and correlation analysis to probe interregional connectivity in fmri task activation datasets. *Magnetic resonance imaging, 18*, 921-930.

Arslan, S., Ktena, S. I., Makropoulos, A., Robinson, E. C., Rueckert, D., & Parisot, S. (2018). Human brain mapping: A systematic comparison of parcellation methods for the human cerebral cortex. *NeuroImage, 170*, 5-30.

Bellec, P., Rosa-Neto, P., Lyttelton, O. C., Benali, H., & Evans, A. C. (2010). Multi-level bootstrap analysis of stable clusters in resting-state fmri. *NeuroImage, 51*, 1126-1139.

Bzdok, D., Varoquaux, G., Grisel, O., Eickenberg, M., Poupon, C., & Thirion, B. (2016). Formal models of the network co-occurrence underlying mental operations. *PLOS Computational Biology, 12*, e1004994.

Damascelli, M., Woodward, T. S., Sanford, N., Zahid, H. B., Lim, R., Scott, A., & Kramer, J. K. (2021). Multiple functional brain networks related to pain perception revealed by fmri. *Neuroinformatics*.

Fedorenko, E., Duncan, J., & Kanwisher, N. (2013). Broad domain generality in focal regions of frontal and parietal cortex. *Proceedings of the National Academy of Sciences, 110*, 16616-16621.

Glasser, M. F., Coalson, T. S., Robinson, E. C., Hacker, C. D., Harwell, J., Yacoub, E., Ugurbil, K., Andersson, J., Beckmann, C. F., Jenkinson, M., Smith, S. M., & Van Essen, D. C. (2016). A multi-modal parcellation of human cerebral cortex. *Nature, 536*, 171-178.

Gordon, E. M., Laumann, T. O., Adeyemo, B., Huckins, J. F., Kelley, W. M., & Petersen, S. E. (2016). Generation and evaluation of a cortical area parcellation from resting-state correlations. *Cerebral Cortex, 26*, 288-303.

Henson, R. N., Rugg, M. D., & Friston, K. J. (2001). The choice of basis functions in event-related fmri. *NeuroImage, 13*, 149-149.

Hunter, M. A., & Takane, Y. (2002). Constrained principal component analysis: Various applications. *Journal of Educational and Behavioral Statistics, 27*, 105-145.

Krienen, F. M., Yeo, B. T. T., & Buckner, R. L. (2014). Reconfigurable task-dependent functional coupling modes cluster around a core functional architecture. *Philosophical Transactions of the Royal Society B: Biological Sciences, 369*, 20130526.

Larivière, S., Lavigne, K. M., Woodward, T. S., Gerretsen, P., Graff-Guerrero, A., & Menon, M. (2017). Altered functional connectivity in brain networks underlying self-referential processing in delusions of reference in schizophrenia. *Psychiatry Research: Neuroimaging, 263*, 32–43.

Lavigne, K. M., Menon, M., Moritz, S., & Woodward, T. S. (2020). Functional brain networks underlying evidence integration and delusional ideation. *Schizophr Res, 216*, 302-309.

Lavigne, K. M., Metzak, P. D., & Woodward, T. S. (2015). Functional brain networks underlying detection and integration of disconfirmatory evidence. *NeuroImage, 112*, 138-151.

Lindquist, M. A., Meng Loh, J., Atlas, L. Y., & Wager, T. D. (2009). Modeling the hemodynamic response function in fmri: Efficiency, bias and mis-modeling. *NeuroImage, 45*, S187-S198.

Metzak, P. D. (2017). *Multimodal examination of brain networks involved in attentional biasing in schizophrenia.* University of British Columbia.

Metzak, P. D., Feredoes, E., Takane, Y., Wang, L., Weinstein, S., Cairo, T. A., Ngan, E. T., & Woodward, T. S. (2011). Constrained principal component analysis reveals functionally connected load-dependent networks involved in multiple stages of working memory. *Human brain mapping, 32*, 856-871.

Metzak, P. D., Riley, J. D., Wang, L., Whitman, J. C., Ngan, E. T., & Woodward, T. S. (2012). Decreased efficiency of task-positive and task-negative networks during working memory in schizophrenia. *Schizophrenia bulletin, 38*, 803-813.

Percival, C., Zahid, H., & Woodward, T. S. (2020). Set of task-based functional brain networks derived from averaging results of multiple fmri-cpca studies (2020 ed., pp. https://zenodo.org/record/4274841#.YFkcXp4274841KhPY). Zenodo.

Poldrack, R. A., Congdon, E., Triplett, W., Gorgolewski, K. J., Karlsgodt, K., Mumford, J., Sabb, F., Freimer, N., London, E., & Cannon, T. (2016). A phenome-wide examination of neural and cognitive function. *Scientific data, 3*.

Roes, M., Chinchani, A., & Woodward, T. S. (2021). Reduced functional connectivity in brain networks underlying paired associates memory encoding in schizophrenia. *Biological Psychiatry: Cognitive Neuroscience and Neuroimaging*.

Sanford, N., Whitman, J. C., & Woodward, T. S. (2020). Task-merging for finer separation of functional brain networks in working memory. *Cortex, 125*, 246-271.

Schaefer, A., Kong, R., Gordon, E. M., Laumann, T. O., Zuo, X.-N., Holmes, A. J., Eickhoff, S. B., & Yeo, B. T. T. (2018). Local-global parcellation of the human cerebral cortex from intrinsic functional connectivity mri. *Cerebral Cortex, 28*, 3095-3114.

Serences, J. T. (2004). A comparison of methods for characterizing the event-related bold timeseries in rapid fmri. *Neuroimage, 21*, 1690-1700.

Smith, S. M., Fox, P. T., Miller, K. L., Glahn, D. C., Fox, P. M., Mackay, C. E., Filippini, N., Watkins, K. E., Toro, R., Laird, A. R., & Beckmann, C. F. (2009). Correspondence of the brain's functional architecture during activation and rest. *Proc Natl Acad Sci U S A, 106*, 13040-13045.

Smith, S. M., Miller, K. L., Moeller, S., Xu, J., Auerbach, E. J., Woolrich, M. W., Beckmann, C. F., Jenkinson, M., Andersson, J., & Glasser, M. F. (2012). Temporally-independent functional modes of spontaneous brain activity. *Proceedings of the National Academy of Sciences, 109*, 3131-3136.

Takane, Y., & Hunter, M. A. (2001). Constrained principal component analysis: A comprehensive theory. *Applicable Algebra in Engineering, Communication and Computing, 12*, 391-419.

Takane, Y., & Shibayama, T. (1991). Principal component analysis with external information on both subjects and variables. *Psychometrika, 56*, 97-120.

Whitman, J. C., Metzak, P. D., Lavigne, K. M., & Woodward, T. S. (2013). Functional connectivity in a frontoparietal network involving the dorsal anterior cingulate cortex underlies decisions to accept a hypothesis. *Neuropsychologia, 51*, 1132-1141.

Whitman, J. C., Takane, Y., Cheung, T., Moiseev, A., Ribary, U., Ward, L., & Woodward, T. S. (2016). Acceptance of evidence-supported hypotheses generates a stronger signal from an underlying functionally-connected network. *NeuroImage, 127*, 215-226.

Wong, S. T. S., Goghari, V. M., Sanford, N., Lim, R., Clark, C., Metzak, P. D., Rossell, S. L., Menon, M., & Woodward, T. S. (2020). Functional brain networks involved in lexical decision. *Brain Cogn, 138*, 103631.

Woodward, T. S., Cairo, T. A., Ruff, C. C., Takane, Y., Hunter, M. A., & Ngan, E. T. (2006). Functional connectivity reveals load dependent neural systems underlying encoding and maintenance in verbal working memory. *Neuroscience, 139*, 317-325.

Woodward, T. S., Tipper, C. M., Leung, A. L., Lavigne, K. M., Sanford, N., & Metzak, P. D. (2015). Reduced functional connectivity during controlled semantic integration in schizophrenia: A multivariate approach. *Human brain mapping, 36*, 2948-2964.

Yarkoni, T., Poldrack, R. A., Nichols, T. E., Van Essen, D. C., & Wager, T. D. (2011). Large-scale automated synthesis of human functional neuroimaging data. *Nature Methods, 8*, 665-670.

Yeo, B. T. T., Krienen, F. M., Eickhoff, S. B., Yaakub, S. N., Fox, P. T., Buckner, R. L., Asplund, C. L., & Chee, M. W. (2015). Functional specialization and flexibility in human association cortex. *Cereb Cortex, 25*, 3654-3672.

Yeo, B. T. T., Krienen, F. M., Sepulcre, J., Sabuncu, M. R., Lashkari, D., Hollinshead, M., Roffman, J. L., Smoller, J. W., Zöllei, L., & Polimeni, J. R. (2011). The organization of the human cerebral cortex estimated by intrinsic functional connectivity. *Journal of neurophysiology, 106*, 1125-1165.

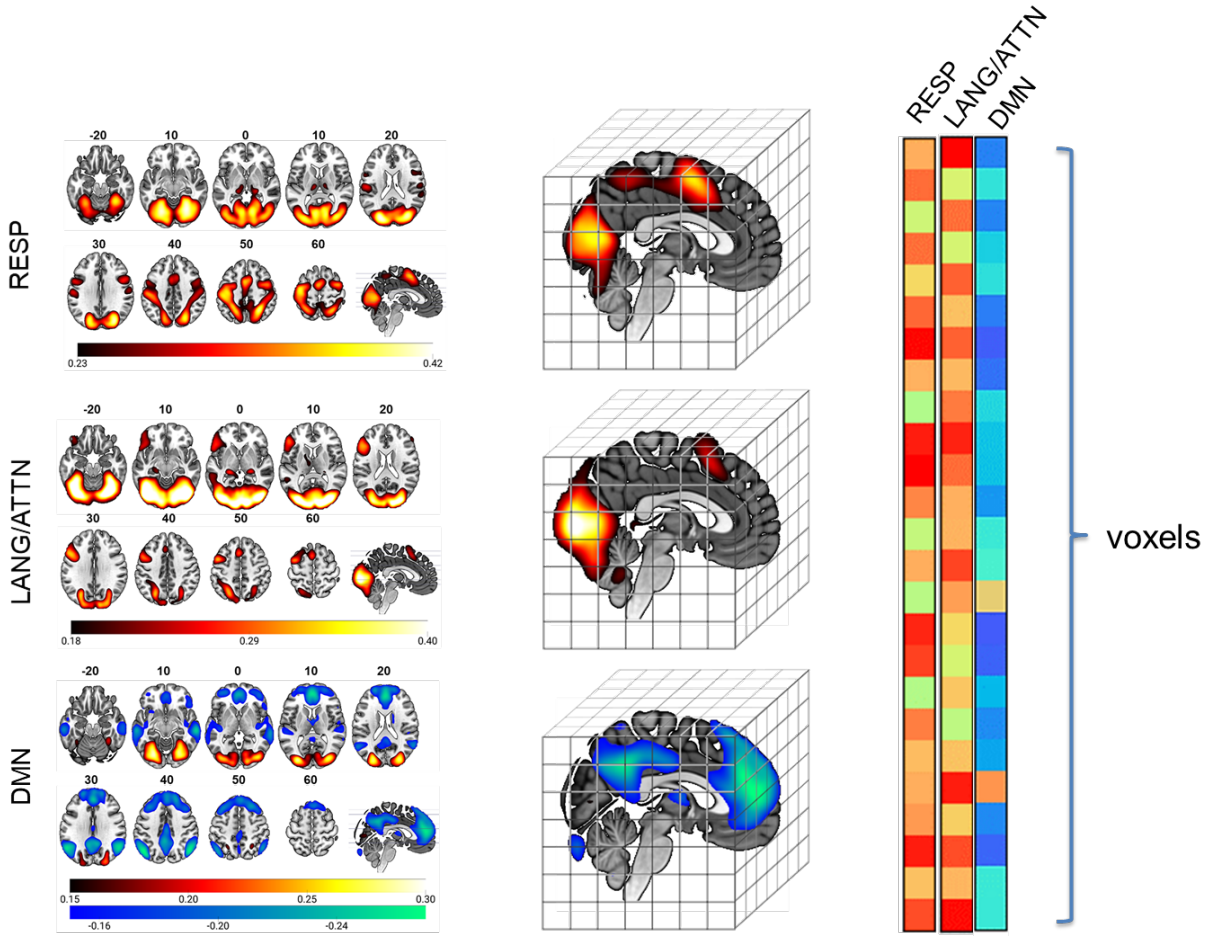


**Figure 1.** Illustration of *H* matrix creation for use in ST-fMRI-CPCA. In this example which illustrates the creation of the *H* matrix for test case 1, the data-driven RESP, LANG/ATTN, and DMN networks from previous work (Roes et al., 2021; in the left panel, shown overlaid onto a brain template) together comprise the spatial model of interest (SMoI). The matrix representation of this spatial model, *H*, is created by transforming the three-dimensional whole-brain network image of intensity values (shown in simplified form in the middle panel) into vectors of length *m* voxels, and horizontally concatenating the vectors. The resulting *H* matrix (shown in simplified form in the right panel) contains a set of columns corresponding to each of the networks included in the SMoI. An additional column of 1's can also be added in order to estimate the intercept (not pictured).

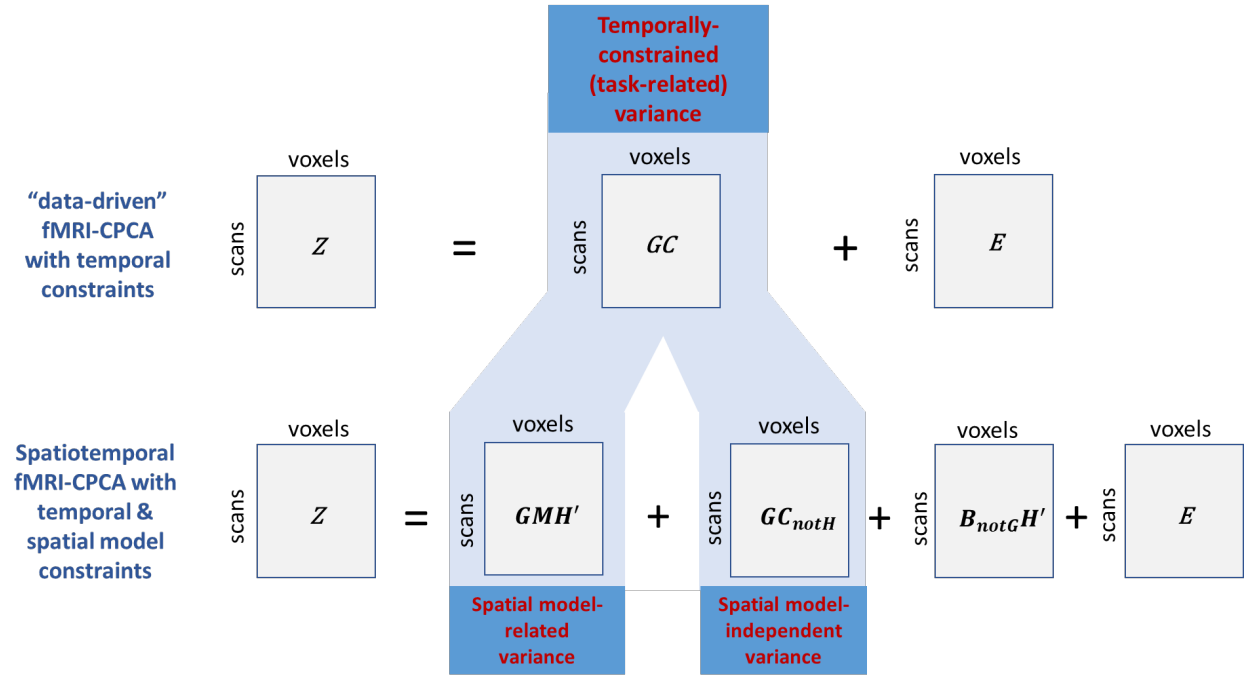


**Figure 2.** Illustration of relation of "data-driven" fMRI-CPCA with temporal constraints only to ST-fMRI-CPCA, which additionally uses spatial constraints. In data-driven analyses, task timing-related variance ($GC$) is isolated by regressing $Z$ onto temporal constraints (task timing information) specified in $G$. In ST-fMRI-CPCA, the $GC$ variance is further subdivided into the task timing-related variance that is predicted by a spatial model ($GMH'$), and the task timing-related variance not predicted by a spatial model ($GC_{notH}$). PCA is then used to dimensionally characterize the spatiotemporal features of each subset of task timing-related variance.

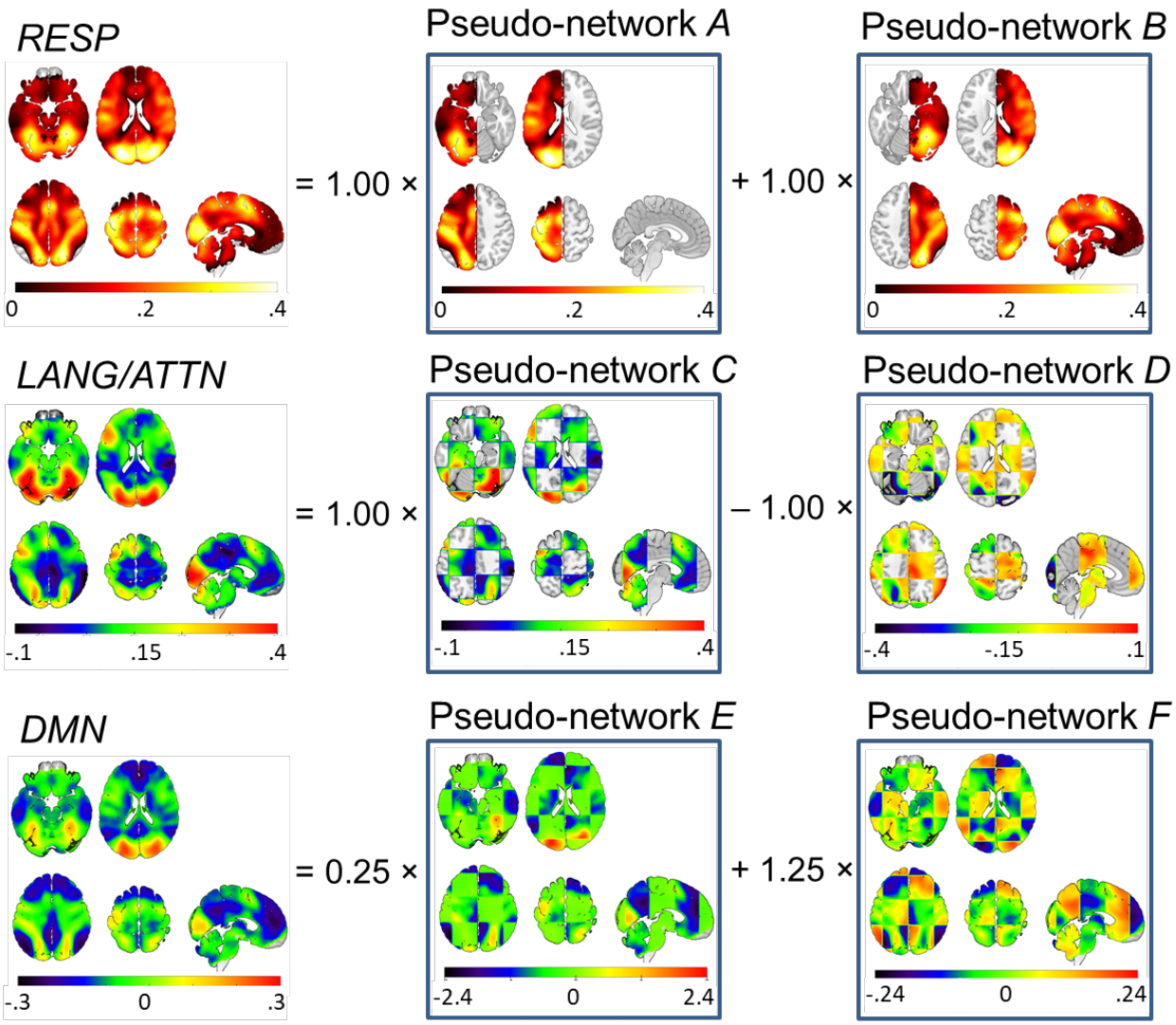


**Figure 3.** Illustration of the pseudo-networks *A*-*F* that were included in the $\boldsymbol{H}$ matrix for test case 3. Pseudo-networks *A*-*F* linearly recombine with weights of [1.0, 1.0, 0.0, 0.0, 0.0, and 0.0], respectively to produce the original data-driven RESP network. Pseudo-networks *A*-*F* linearly recombine with weights of [0.0, 0.0, 1.0, -1.0, 0.0, and 0.0] respectively, to produce the original data-driven LANG/ATTN network. Pseudo-networks *A*-*F* linearly recombine with weights of [0.0, 0.0, 0.0, 0.0, 0.25, and 1.25] respectively, to produce the original data-driven DMN. Therefore, in the quality control demonstration of test case 3, these are the expected $P_H$ values for the three $\boldsymbol{GMH'}$ components estimating the data-driven networks.

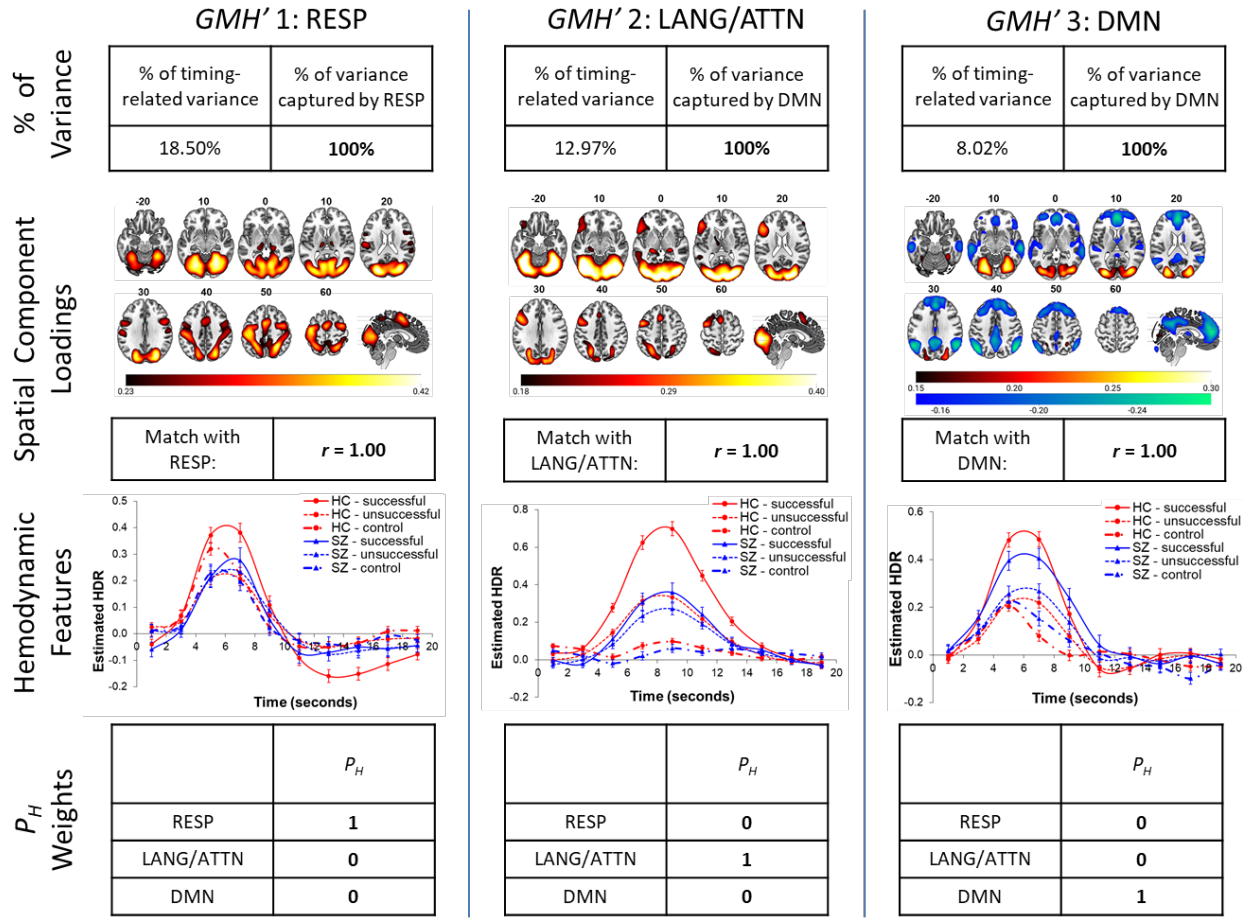


**Figure 4.** Visual summary of the results of ST-fMRI-CPCA test case 1. In this test case, all data-driven networks were included in $\boldsymbol{H}$. Each vertical panel represents a distinct component of $\boldsymbol{GMH}'$ and demonstrates that the task timing-related variance captured, spatial features (component loadings), and hemodynamic features of each $\boldsymbol{GMH}'$ component corresponded to the data-driven networks that were included in $\boldsymbol{H}$. Spatial correspondence between the data-driven and spatial model-estimated networks were assessed using Fisher-transformed spatial correlation with df = 4000 ($\boldsymbol{Z}$ values in parentheses). The final row shows the spatial model weights indicating how the spatial predictors in $\boldsymbol{H}$ linearly recombine to produce the $\boldsymbol{GMH}'$ component image estimating the task-based network.

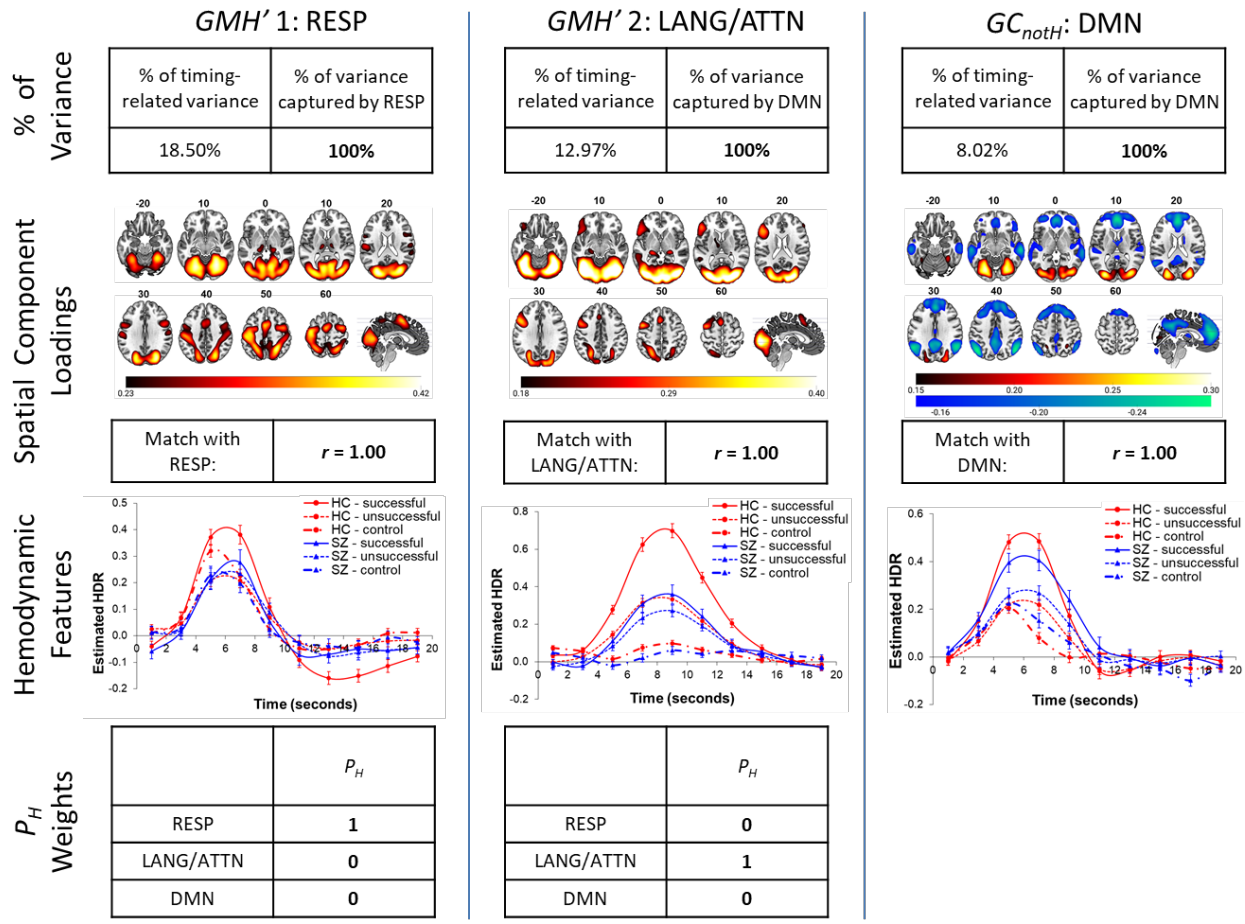


**Figure 5.** Visual summary of the results of test case 2. In this test case, the RESP and LANG/ATTN data-driven networks were included in $\boldsymbol{H}$, but the DMN was excluded. The left and middle vertical panels represent two distinct components of $\boldsymbol{GMH'}$, and the right panel represents a single $\boldsymbol{GC_{notH}}$ component. Examination of the variances captured, the spatial features (component loadings and spatial correlations), and the hemodynamic features of each component shows that the two $\boldsymbol{GMH'}$ components exactly correspond to the data-driven networks included in $\boldsymbol{H}$ (RESP and LANG/ATTN), and the $\boldsymbol{GC_{notH}}$ component exactly corresponds to the DMN. The final row shows the spatial model weights specifying how the spatial predictors in $\boldsymbol{H}$ linearly recombine to produce the $\boldsymbol{GMH'}$component image. (Note that $\boldsymbol{GC_{notH}}$ components do not have spatial model weights, as they are independent from spatial model constraints).

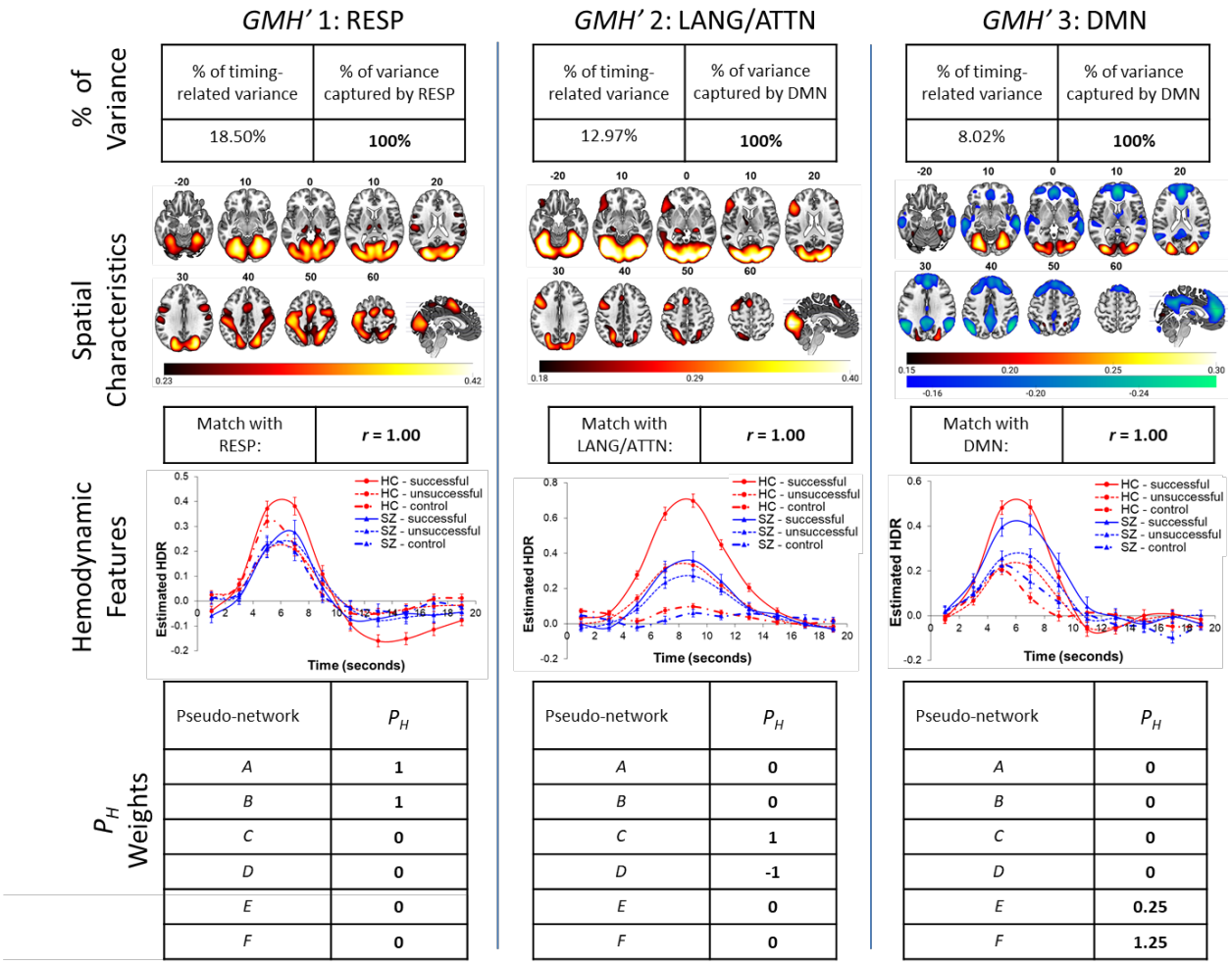


**Figure 6.** Visual summary of the results of test case 3. In this test case, six pseudo-networks that linearly recombined to produce the RESP network, LANG/ATTN, and DMN were included in $\boldsymbol{H}$ as specified previously in Figure 3. Each vertical panel represent a distinct $\boldsymbol{GMH'}$ component. Examination of the variances captured, the spatial features (component loadings and spatial correlations), and the hemodynamic features of each component shows that the $\boldsymbol{GMH'}$ components exactly corresponded to the data-driven RESP, LANG/ATTN and DMN. The final row of this image shows the spatial model weights specifying how the spatial predictors in *H* linearly recombined to produce each $\boldsymbol{GMH'}$component image. These values were as predicted and therefore validate that our ST-fMRI-CPCA program works as expected.

Supplementary Information

# Combining temporal and spatial constraints in task-based fMRI

Meighen Roes[1,2]

Yoshio Takane[3]

&

Todd S. Woodward[2,4*]

[1]Department of Psychology, University of British Columbia, Vancouver, BC, Canada.

[2]BC Mental Health and Substance Use Research Institute, Provincial Health Services Authority, Vancouver, BC, Canada.

[3] Department of Psychology, University of Victoria, Victoria, Canada

[4]Department of Psychiatry, University of British Columbia, Vancouver, BC, Canada.

*Corresponding author. Please address correspondence to Todd S. Woodward, Ph.D., BC Mental Health and Substance Use Research Institute, Room 117, 3rd Floor, 938 W. 28th Avenue, Vancouver, B.C., Canada. V5Z 4H4. E-mail: todd.woodward@ubc.ca. Phone: 604-875-2000 x 4724. Fax: 604-875-3871.

## Methods

### *Data-driven fMRI-CPCA:*

#### *Step 1: Multivariate Multiple regression*

In the first step of a data-driven fMRI-CPCA analysis, multivariate least-squares linear regression is carried out. In this step, the data matrix of voxel activations across all scans ($Z$) (after masking out non-brain areas, and realigning, smoothing, spatially normalizing, mean-centering and standardizing to a variance of 1.0) is regressed onto the task timing/design matrix ($G$):

$$Z = GC + E,$$

where $C$, the matrix of condition-specific regression weights, is

$$C = (G' \times G)^{-1} \times G' \times Z,$$

and $GC$ contains variability in $Z$ predictable from the design matrix $G$ (i.e., the variability in BOLD signal predictable from the timing of stimulus presentations.)

#### *Step 2: Principal Component Analysis of task-specific variance*

In the second step of data-driven fMRI-CPCA, the matrix $GC$ is subjected to singular value decomposition (SVD) to identify patterns of intercorrelated whole-brain voxel activity that are predictable from stimulus onset timing. Each component that results from this decomposition represents a potential functional network:

$$UDV' = GC$$

In the decomposition, the left singular vector $U$ contains time-series information about the components; $D$ is the diagonal matrix of singular values that, when squared, are proportional to the variances explained by each component; The right singular vector $V$ contains spatial information about the components, and can be rescaled, $\frac{VD}{\sqrt{m-1}}$, to produce component loadings

for each voxel. Component loadings can be overlaid onto a structural brain image to represent the spatial topography of the task-timing related functional network.

Next, a matrix of predictor weights $P$ (the weights when applied to $G$ to produce $U$) is computed as the regression weights predicting $U$ from $G$. Predictor weights indicate the importance of each column in $G$ (i.e., each modeled post-stimulus timepoint for each subject and condition) to the temporal information about the brain network represented in $U$. Those columns in *G* that contribute most strongly to the variation over time captured in $U$ correspond to the peaks of the hemodynamic response. As a result, the fMRI-CPCA approach estimates a hemodynamic response (HDR) shape for each individual and condition separately, allowing us to interpret each network with respect to the conditions modeled in the design matrix $G$.

Predictor weights can be entered into repeated-measures ANOVA to assess for the reliability of the hemodynamic response. A significant effect of post-stimulus time, along with a biologically plausible HDR shape, indicates that the network exhibits a reliable BOLD response. Group- and condition-related effects in estimated BOLD activity can also be tested using RM ANOVA.

*Spatiotemporal fMRI-CPCA: Computation and Characterization of task timing-unrelated portions of variance*

$B_{notG}H'$ represents the portion of $Z$ that can be explained by $H$ independent of $G$. In fMRI-CPCA, this corresponds to the BOLD signal variance that is independent of task timing but predictable from the spatial model (i.e., task-unrelated fluctuations in the model's networks over the course of the scanning session). The parameter $B_{notG}$ is the matrix of spatial model regression weights for the regression of $Z$ onto that part of $H$ that is independent of $G$:

$$B_{notG} = [I_{n\times s} - G \times (G' \times G)^{-1} \times G'] \times Z \times H \times (H' \times H)^{-1},$$

where $I_{n\times s}$ is an identity matrix sized on the rows of $Z$ (n subjects × s scans) that contains ones on the main diagonal and zeros elsewhere.

Should a researcher have interest in characterizing this portion of the variance, the matrix. $B_{notG}H'$would also be decomposed through principal component analysis as previously described. In this case, the spatial model weights $P_{HnotG}$ represent the unstandardized beta coefficients produced by regressing the right singular vector of $B_{notG}H'$ onto $H$. No timing-related predictors would be produced estimating the HDR, because this portion of variance is not predictable from task timing.

Finally, the last term in the full CPCA model, $E$, is the error term – i.e., the variance in $Z$ that cannot be estimated by $G$, $H$ or the interaction of $G$ and $H$:

$$E = Z - GMH' - B_{notG}H' - GC_{notH}.$$

*Supplementary Details regarding creation of Pseudo-networks for Test Case 3*

*Pseudo-networks C and D:*

To create Pseudo-networks *C* and *D*, we first created a three-dimensional checkerboard pattern in the same space as our brain scan images. Pseudo-network $C$ was created by taking the natural LANG/ATTN loadings wherever the checkerboard had a value of 1.00; Pseudo-network $D$ consisted of the remaining natural LANG/ATTN loadings (where the checkerboard had a value of 0.00), multiplied by -1. As a result, subtracting Pseudo-network $D$ from Pseudo-network $C$ produced the original LANG/ATTN loadings, such that $LANG/\,ATTN = (1.00 \times C) + (-1.00 \times D)$.

*Pseudo-networks E and F:*

To produce Pseudo-network *F*, the natural DMN component loadings for any voxels having a value of 1.00 in the checkerboard image were inverted (multiplied by -1.00), and the resulting image was rescaled by dividing all voxel values by 1.25. Then, Pseudo-network *E* was solved for such $DMN = (1.25 \times E) + (0.25 \times F)$, using linear matrix algebra in MATLAB.